Available online at www.sciencedirect.com
SCIENCE DIRECT®
Journal of Molecular Catalysis A: Chemical 227 (2005) 25–35
JOURNAL OF MOLECULAR CATALYSIS A: CHEMICAL
www.elsevier.com/locate/molcata

Catalytic reduction of NO_2 in nanocrystalline NaY zeolite

Gonghu Li, Sarah C. Larsen**, Vicki H. Grassian*

Department of Chemistry, The University of Iowa, Iowa City, IA 52242, USA

Received 30 July 2004; received in revised form 3 October 2004; accepted 4 October 2004
Available online 18 November 2004

Abstract

In this study, in situ transmission FT-IR spectroscopy was employed to investigate the thermal and selective catalytic reduction of NO_2 with propylene in nanocrystalline NaY zeolite. NO was the major product in the thermal reduction of NO_2. In absence of oxygen and water, selective catalytic reduction of NO_2 with propylene at low temperatures ($T \leq 473$ K) resulted in the complete reduction of NO_2 to N_2 and O_2. Isocyanate and nitrile species formed on extra framework alumina sites are found to be important intermediates. Based on kinetic studies, a pathway involving radical reactions appears to be the most plausible mechanism for the complete reduction of NO_2.

Keywords: Selective catalytic reduction; NO_2; Y zeolite; Propylene; Nanoparticles

1. Introduction

The emission control of nitrogen oxides (NO_x) from engine exhaust is of great importance due to their contribution to processes harmful to the environment [1–3]. Selective catalytic reduction (SCR) of NO_x with NH_3 or hydrocarbons (HCs) has emerged as an effective technology using oxide and zeolite based catalysts [4–6]. Zeolites are considered particularly promising SCR catalysts because of their cation exchange capacity and acid–base properties.

Several recent studies have investigated alkali and alkaline earth-exchanged Y, FAU zeolites in the adsorption and HC-SCR of NO_x [7–14]. NO_2 can be stored in zeolite Y in the form of stable nitrate and nitrite species. The adsorption of NO_2 (or $NO + O_2$) in zeolite Y has been suggested to proceed via the disproportionation of N_2O_4 or the reaction of NO_2 with the residual water in zeolite. As for the mechanism of HC-SCR, previous studies have suggested isocyanates to be key intermediates in this reaction [15,16]. Organic nitro/nitrito compounds are first generated in the reaction between adsorbed hydrocarbons and surface nitrate/nitrite species. These compounds are then converted to isocyanates. Isocyanates will react with NO_x from the gas phase producing dinitrogen. Although the general reaction scheme can be understood from these steps, many details still remain elusive, such as the mechanism for the formation of the nitrogen–nitrogen bond in complete reduction. Ammonium ions or free radicals have been proposed as key intermediates in the formation of dinitrogen [7,17].

Most HC-SCR studies in zeolites have been carried out at temperatures above 673 K. At these elevated temperatures, many side reactions can take place [3]. In this study, thermal reduction and propylene-SCR of NO_2 were done at lower temperatures ($T \leq 473$ K) and monitored with in situ FT-IR spectroscopy. Infrared spectroscopy has been widely used to investigate the adsorption and the selective catalytic reduction of NO_x [18–22]. In particular, information concerning the kinetics and mechanism of these reactions may be discerned from this spectroscopic technique. In addition, synthesized nanocrystalline NaY zeolite was used as the catalyst instead of commercially available zeolite catalysts. As discussed in a recent publication, nanocrystalline zeolites may be particularly useful in environmental applications due to

* Corresponding author. Tel.: +1 319 335 1392; fax: +1 319 335 1270.
** Co-corresponding author.
E-mail addresses: sarah-larsen@uiowa.edu (S.C. Larsen), vicki-grassian@uiowa.edu (V.H. Grassian).

1381-1169/$ – see front matter © 2004 Elsevier B.V. All rights reserved.
doi:10.1016/j.molcata.2004.10.002

the small particle size and large internal and external surface areas [23,24].

2. Experimental

2.1. Zeolite sample preparation and materials

Nanocrystalline NaY zeolite was synthesized according to methods described in the literature [25]. Two solutions (A and B) were prepared. Solution A was obtained by dissolving NaOH and tetramethylammonium hydroxide (TMAOH) in distilled water and then adding aluminum isopropylate to the alkali solution. Solution B was prepared by adding tetraethyl orthosilicate (TEOS) to the remainder of the TMAOH solution. Both solutions were filtered through a 0.2 μm filter paper, then mixed together and stirred overnight at room temperature. The clear solution mixture obtained was then heated in a Teflon-lined stainless steel autoclave for 3 days at 403 K. The resulting solution was centrifuged for 30 min at 3400 rmp. The product was washed with distilled water and dried in air.

The synthesized zeolite was characterized using powder X-ray diffraction (Siemans D5000) to assess the crystallinity and to verify the identity of the zeolite. Scanning electron microscopy (SEM, Hitachi S-4000) was used to determine particle morphology and particle size. The average particle size was determined to be 80 ± 30 nm from SEM. The surface area was measured on an automated Quantachrome Nova 1200 multipoint BET apparatus. The internal and external surface areas of the synthesized zeolite were 474 and 46 $m^2\,g^{-1}$, respectively. Based on previous work [26], the particle size of the zeolite was calculated using the external surface area to be approximately 88 nm, in reasonable agreement with the SEM measurement. ^{27}Al and ^{29}Si magic angle spinning (MAS) NMR (300 MHz wide bore, Tecmag) were performed on the sample. NMR signals from tetrahedral Al and Si atoms were identified. The Si/Al ratio was determined to be 1.7 from ^{29}Si MAS NMR.

Research-grade purity oxygen and carbon dioxide were purchased from Air Products. Research-grade purity nitrogen dioxide, propylene, nitric oxide, nitrous oxide and carbon monoxide from Matheson. All gases were used as received. Pyridine (99.9%) was purchased from Fisher Scientific. Pyridine was further dehydrated over molecular sieves and purified before use by several freeze-pump-thaw cycles.

2.2. Fourier transform infrared spectroscopy

The infrared sample cell used in this study has been described previously [27]. Approximately 8 mg of NaY zeolite mixed with some water were coated onto a 3 cm × 2 cm photoetched tungsten grid held in place by nickel jaws. The nickel jaws are attached to copper leads so that the sample can be resistively heated. A thermocouple wire attached to the tungsten grid is used to measure the temperature of the sample. The tungsten grid with zeolite sample is placed inside of a stainless steel cube. The cube has two BaF_2 windows for infrared measurements and is connected to a vacuum/gas handling system.

The stainless steel IR cell is held in place by a linear translator inside the sample compartment of a Mattson Galaxy 6000 infrared spectrometer equipped with a narrow-band MCT detector. The linear translator allows each half of the sample grid to be translated into the infrared beam. This permits the detection of gas phase and adsorbed species in zeolites under identical reaction conditions. Each spectrum was obtained by averaging 64 scans at an instrument resolution of 4 cm^{-1}. Each absorbance spectrum shown represents a single beam scan referenced to the appropriate single beam scan of the clean zeolites or the blank grid, unless otherwise noted.

The NaY sample was gradually heated under vacuum at 573 K or higher temperature overnight to remove adsorbed water. Reactant gases were loaded into the zeolite through the gas handling system. Two absolute pressure transducers were used to monitor the pressures. Typically, the zeolite was equilibrated with each gas prior to a spectrum being recorded. In pyridine adsorption experiments, adsorption was carried out by equilibrating the zeolite powder with 1 Torr pressure of pyridine vapor at room temperatures. The sample was then evacuated for 30 min before a spectrum was recorded. The desorption of pyridine was monitored by evacuating the sample for 30 min at elevated temperatures and cooling back to room temperature prior to recording a spectrum.

In SCR reactions, NO_2 and propylene (1:1 ratio) were pre-mixed in a chamber before being introduced into the IR cell at room temperature. Time course experiments were conducted by automatically scanning the gas phase every 2 min. The extinction coefficient of individual gases was calibrated using the characteristic IR absorption bands and measuring the pressure using an absolute pressure transducer. Assuming ideal gas behavior, the amount of gas can be calculated from its pressure and volume of the IR cell.

3. Results

3.1. An investigation of the nature of the surface sites on nanocrystalline NaY

Five absorption bands due to hydroxyl groups were identified in the infrared spectra after heating the NaY zeolite overnight under vacuum at temperatures of 573 and 673 K, as shown in Fig. 1. Although there is an overall decrease in intensity of the band in this region after heating from 573 to 673 K, the five absorption bands are still evident at 673 K. The relatively intense high frequency absorption band at 3745 cm^{-1} is assigned to terminal silanol groups that are on the external surface of the particles. This feature is of much weaker intensity in a commercial sample of NaY zeolite that has a much larger particle size [23]. Thus, this result

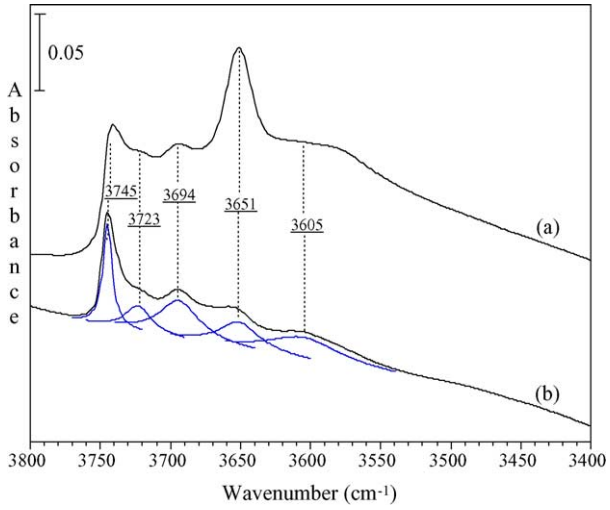

Fig. 1. FT-IR spectra of surface hydroxyl groups in nanocrystalline NaY zeolite after heating to (a) 573 K and (b) 673 K overnight under vacuum. The two spectra were recorded at $T = 298$ K. Five different O–H groups were identified in the spectrum. The spectrum recorded after heating to 673 K overnight is fit to five bands with Lorentzian line-shapes so that these bands can be more readily discerned. The blank grid is used as a reference.

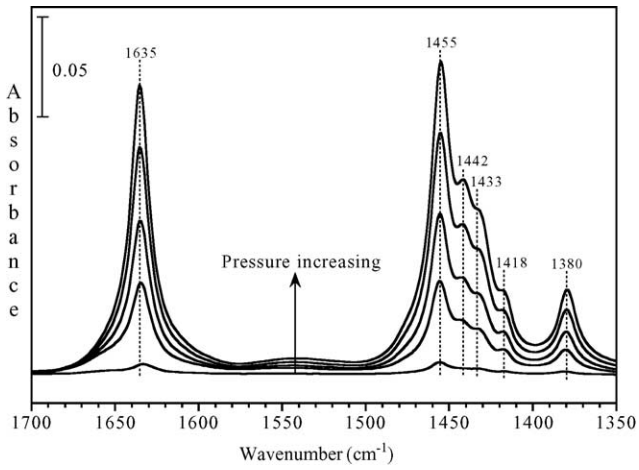

Fig. 2. FT-IR spectra of propylene adsorbed in nanocrystalline NaY zeolite at $T = 298$ K as a function of propylene pressure ($P = 0.050$, 0.493, 1.019, 2.028 and 4.061 Torr). All spectra shown in Fig. 2 use the clean nanocrystalline NaY zeolite prior to adsorption as a reference. In addition, gas-phase absorptions have been subtracted from each of the FT-IR spectra.

confirms that the synthesized NaY zeolite consists of small particles. The next highest frequency absorption band around 3723 cm^{-1} is associated with hydroxyl groups occurring at defect sites (also called hydroxyl nests) [28]. The absorption band at 3694 cm^{-1} has been assigned to surface hydroxyl groups near Na^+ sites, while the bands at 3654 and 3605 cm^{-1} are associated with hydroxyl group attached to extra framework alumina (EFAL) species [29,30] and adsorbed water, respectively.

Several probe molecules were used to detect the presence of additional surface adsorption sites for the synthesized nanocrystalline zeolite Y used in this study. The adsorption of propylene in NaY (see Fig. 2) results in an absorption band at 1635 cm^{-1} assigned to the C=C stretching mode and several bands between 1350 and 1500 cm^{-1} associated with the CH_3 deformation mode and the CH_2 scissor mode. Absorptions due to C–H stretching modes between 2800 and 3100 cm^{-1} were also observed (not shown). All of the absorption features disappeared after evacuation of gas-phase propylene at room temperature for several minutes. With excess propylene in the IR cell, no pronounced change of the band at 1635 cm^{-1} was observed at room temperature for 6 h, indicating that propylene did not undergo polymerization in the nanocrystalline NaY zeolite. It can therefore be concluded that strong Bronsted acid sites that initiate propylene polymerization are not present in the nanocrystalline NaY zeolite pretreated at 573 K [31]. The FT-IR spectra shown in Fig. 1 are consistent with this conclusion as strong Bronsted acid sites are typically bridging OH groups with vibrational frequencies of 3630 and 3560 cm^{-1} [29,32]. These bands are not observed in the infrared spectra of nanocrystalline NaY shown in Fig. 1.

Pyridine adsorption, however, revealed the existence of weaker Bronsted acid sites as well as Lewis acid sites in the NaY zeolite. It is well known that weakly adsorbed pyridine with characteristic vibrational frequencies of 1617, 1592, 1574 and 1441 cm^{-1} desorbs near 470 K [32,33]. In contrast, pyridinium ions with characteristic vibrational frequencies of 1632 and 1545 cm^{-1} generated by reaction with Bronsted acid sites desorb at much higher temperatures. Similarly, pyridine molecules that adsorbed at Lewis acid sites are also more strongly adsorbed. Pyridine molecules adsorbed at Lewis acid sites can be identified from characteristic absorptions at 1621 and 1454 cm^{-1}. All three types of adsorbed pyridine molecules contribute to the absorption band at 1489 cm^{-1}. Fig. 3 displays the FT-IR spectra of pyridine molecules adsorbed in the nanocrystalline NaY zeolite following desorption at three different temperatures (298, 373 and 473 K). It can be seen from the infrared spectrum at 298 K that all three types of adsorbed pyridine molecules are observed. After heating to higher temperatures, only pyridine molecules adsorbed on Bronsted and Lewis acid sites are apparent in the infrared spectra. The Bronsted acid sites may be associated with the surface hydroxyl groups attached to EFAL species.

3.2. Adsorption and thermal reduction of NO_2

The adsorption and reaction of NO_2 on surfaces have been extensively studied due to its environmental importance. FT-IR spectra recorded of the NaY zeolite as a function of NO_2 pressure are shown in Fig. 4. It is evident from the spectra that exposure to NO_2 results in the formation of several surface species whose frequencies fall into two spectral regions: 1200–1660 cm^{-1} due to NO_3^- and NO_2^- 1900–2300 cm^{-1} due to NO^+. Previous studies on nitrogen oxide adsorption make the assignment of the spectra relatively straightforward [34–39]. At low pressures, a doublet with absorbance max-

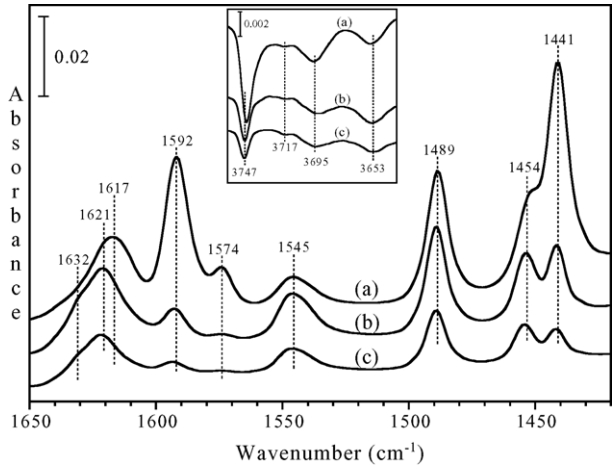

Fig. 3. FT-IR spectra of pyridine molecules adsorbed in nanocrystalline NaY zeolite at $T = 298$ K following pyridine desorption at (a) 298 K, (b) 473 K and (c) 573 K. The inset shows the spectral region extending from 3635 to 3760 cm^{-1}. The spectra were recorded at 298 K. All spectra shown in Fig. 3 use the clean nanocrystalline NaY zeolite prior to adsorption as a reference. In addition, gas-phase absorptions have been subtracted from each of the FT-IR spectra. The peaks in the spectra are assigned to weakly adsorbed pyridine and pyridine adsorbed on acid sites. See text for further details.

ima at 1410 and 1386 cm^{-1} can be attributed to the ν_3 mode splitting of surface nitrate (NO_3^-) adsorbed on Na^+ sites. At higher loading, the doublet converges into a singlet with a frequency of 1407 cm^{-1}. This broadening of the nitrate bands is most likely due to intermolecular interactions [11,12]. The absorption at 1230 cm^{-1} is associated with adsorbed nitrite (NO_2^-). Absorption bands at 1627, 1581 and 1554 cm^{-1} are associated with nitrate absorptions on the EFAL bonded in different coordinations (bridging, bidendate and monodentate, respectively) [2]. The absorption at 1327 cm^{-1} is also associated with nitrate adsorption on EFAL sites.

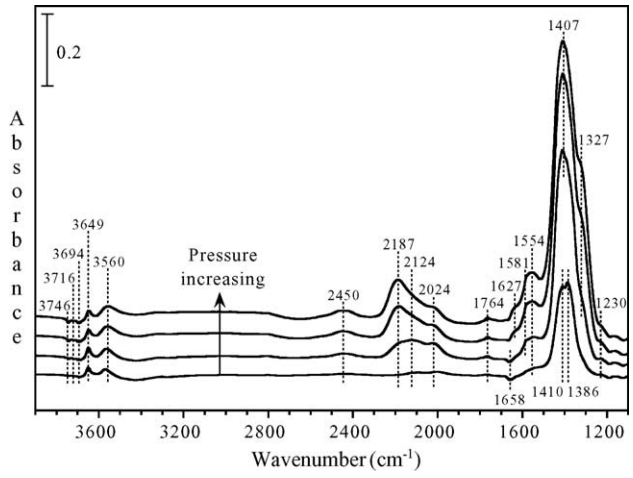

Fig. 4. FT-IR spectra of NO_2 adsorbed in nanocrystalline NaY zeolite at $T = 298$ K as a function of NO_2 pressure ($P = 0.055$, 0.107, 0.498 and 1.033 Torr). All spectra shown in Fig. 4 use the nanocrystalline NaY zeolite prior to adsorption as a reference. In addition, gas-phase absorptions have been subtracted from each of the FT-IR spectra.

The absorption bands within the spectral region between 1900 and 2300 cm^{-1} are assigned to nitrosonium ions (NO^+) [11,40]. At low pressures, two bands at 2024 and 2124 cm^{-1} are due to the formation of NO^+ species adsorbed onto different cationic position in the zeolite framework. At high pressures, an absorption feature at 2187 cm^{-1} develops. This feature can be assigned to the N–O stretching mode from $[NO^+][NO_2]$ or $[NO^+][N_2O_4]$ adducts adsorbed onto Lewis base sites [11,12]. Two other bands at 2450 and 1764 cm^{-1} can be assigned to an overtone and combination bands of adsorbed nitrates [22].

In the hydroxyl group region, loss of three bands at 3694, 3716 and 3746 cm^{-1} was observed because of either the displacement or interaction of hydroxyl groups with adsorbed NO_x^- species. Perturbed hydroxyl groups on EFAL species gave rise to two absorptions at 3649 and 3560 cm^{-1} [12]. At low NO_2 pressure, a negative peak around 1658 cm^{-1} was visible, indicating the consumption of residual H_2O in the zeolite upon NO_2 adsorption.

Thermal reduction of NO_2 at temperatures from 298 to 573 K was investigated. FT-IR spectra of the gas phase were taken at 2 min time intervals. The concentration of the gases in the infrared cell can be determined from the integrated absorbances of the bands at 1616 cm^{-1} (NO_2), 1875 cm^{-1} (NO) and 2224 cm^{-1} (N_2O) using calibrated extinction coefficients. The time course concentration of gas-phase products in thermal reduction of NO_2 at 373 K is shown in Fig. 5. Immediately after heating began, the concentration of NO_2 in the gas phase jumped to a maximum and then decreased quickly. Clearly a large amount of NO_2 was released from the NaY zeolite upon heating, possibly via the reaction of highly active surface nitrate [41]. NO and N_2O were the only other gas-phase products detected by the FT-IR spectroscopy.

The product distribution and conversion of both gaseous NO_2 and adsorbed NO_3^- at three different temperatures are listed in Table 1. In thermal reduction of NO_2, NO was the major product. N_2O accounted for less than 2% of the prod-

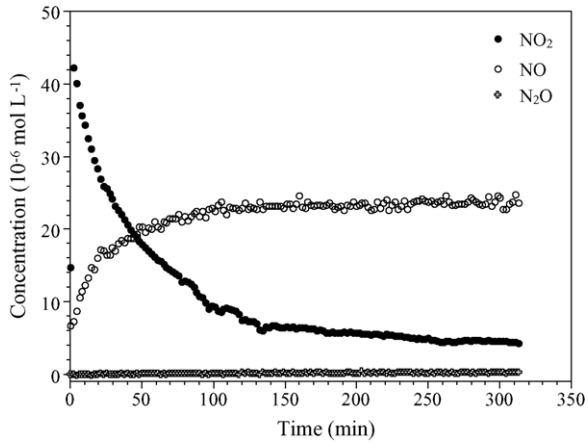

Fig. 5. Time evolution of gas phase NO_2, NO and N_2O during the thermal reduction of NO_2 in nanocrystalline NaY at 373 K. Spectra were recorded every 2 min.

Table 1
Product distribution and conversion of gas-phase NO_2 and adsorbed NO_3^- in the thermal reduction of NO_2 at different temperatures after 6 h of reaction time

Reaction temperature (K)	Gas products (μmol L^{-1})[a]		%Conversion[b]	
	NO	N_2O	NO_2	NO_3^-
298	10.1	0	79	11
373	23.6	0.2	71	64
473	51.3	0.8	92	90

[a] In thermal reduction, the total loading of NO_2 was controlled to be 50 ± 5 μmol L^{-1}; the initial concentration of gas-phase NO_2 after adsorption equilibrium at 298 K was 14 ± 2 μmol L^{-1}.

[b] Conversion of NO_2 refers to change of NO_2 in gas phase; conversion of NO_3^- describes the change associated with the integrated absorbance in the entire 1240–1660 cm^{-1} spectral region.

ucts in the temperature range studied. More than 70% of gas-phase NO_2 decomposed after reaction at 373 K for 6 h. The efficiency reached 100% when the temperature was above 523 K. The concentration of N_2 and O_2 couldn't be monitored in this study. However, based on the nitrogen mass balance, it appears that little N_2 and O_2 were formed in the thermal reduction of NO_2.

In order to measure the thermal stability of the various surface species in the zeolite, NO_2 was first adsorbed in nanocrystalline NaY zeolite at 298 K and the sample was then heated to different temperatures. Fig. 6 shows the FT-IR spectra of surface species adsorbed in NaY zeolite after evacuating the zeolite at different temperatures. Surface adsorbed NO^+ was removed completely by evacuating at 298 K for 30 min, while less than 10% of the original NO_3^- species still remained adsorbed in the zeolite after heating to 573 K. The quantitative study by Sedlmair et al. has shown the relative stability of the NO_x surface species as following: Na^+-nitrates > Al-nitrates > nitrites [12]. In our work, nitrates also appear to be the more stable species relative to nitrites and nitrosonium ions.

Table 2
Assignment of infrared absorption bands observed following adsorption of NO_2 and propylene (1:1) mixture in nanocrystalline NaY zeolite

Bands (cm^{-1})	Assignments	Possible species	Reference
3300–3150	ν(OH)	Oximes	[18,47]
2985	ν(=CH_2)	RCH=CH_2	[42]
2317	ν(NCO)	SiNCO	[43,44]
2272	ν(NCO)	HNCO	[7,44]
2239	ν(NCO)	RNCO	[19,48–52]
2187	ν(CN)	RCN	[48,51,52]
1969	ν(N—O)	NO (a)	[35]
1943	ν(N=O)	N_2O_3 (a)	[35]
1723, 1694	ν(C=O)	Carbonyl species	[7,47]
1647	ν(ONO)	RONO (or $RCONH_2$)	[7,20,21,47]
1598, 1483	–	Carbonaceous species	[46]
1557, 1387	ν(NO_2)	RNO_2	[7,20,21,47]
1528	ν(CO_3^{2-})	Carbonate ion	[42]
1508	ν(COO^-)	Formate ion	[42]
1354	δ(CH_3)	RCH_3	[7]
1282	ν(C—O)	RONO	[45]

3.3. Adsorption of NO_2 and propylene (1:1) mixture

In the propylene-SCR reaction, NO_2 and propylene were pre-mixed (1:1 mole ratio) in a chamber prior to being introduced into the infrared cell. The FT-IR spectra of the resulting mixture adsorbed in NaY zeolite at 298 K are shown in Fig. 7. In comparison to the adsorption of NO_2 alone, similar absorption features were observed in the NO_3^- region. In addition, several new absorption bands were also observed. Assignments of these bands are given in Table 2. Most of

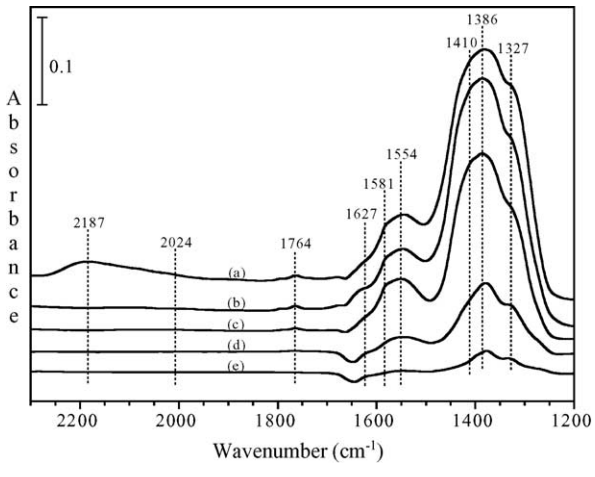

Fig. 6. FT-IR spectra of NO_2 adsorbed in nanocrystalline NaY zeolite after adsorption at (a) 298 K in the presence of the gas phase and (b) after evacuation of the gas phase. The sample was then heated to (c) 373 K, (d) 473 K and (e) 573 K for 30 min. All spectra were recorded at $T = 298$ K. All spectra shown in Fig. 6 use the nanocrystalline NaY zeolite prior to adsorption as a reference. In addition, gas-phase absorptions have been subtracted from each of the FT-IR spectra.

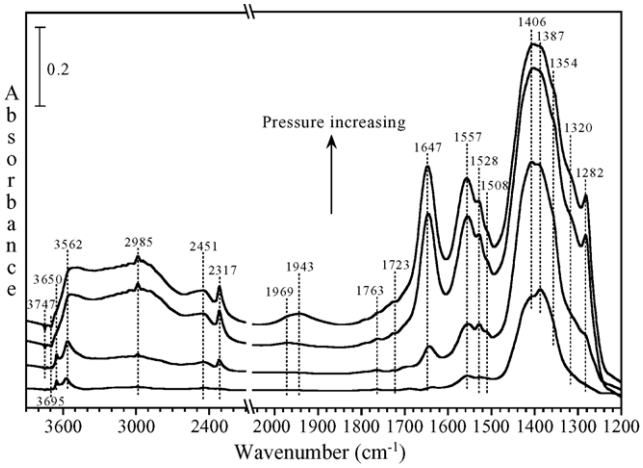

Fig. 7. FT-IR spectra of NO_2 and propylene (1:1) mixture adsorbed in nanocrystalline NaY zeolite at 298 K recorded as a function of increasing total pressure ($P = 0.100$, 0.200, 0.623, 1.005 Torr). All spectra shown in Fig. 7 use the nanocrystalline NaY zeolite prior to adsorption as a reference. In addition, gas-phase absorptions have been subtracted from each of the FT-IR spectra.

these assignments are based on previous studies reported in the literature [42–52].

It is important to note that the spectra contain a wealth of information and there is some considerable overlap of some of the bands in several spectral regions. For example, both Na^+-nitrates and surface adsorbed organic nitro compounds can contribute to the intensity of the observed band at 1387 cm^{-1}. The absorption at 1647 cm^{-1} is assigned to organic nitrito species, but it may also, in part, be due to the formation of carbonyl groups in primary amides or the C=N stretching mode of oximes [47,48]. Therefore, careful analysis of the FT-IR spectra is important in identifying the adsorbates present. Thermal stability of the surface compounds was investigated to assist in making these spectral assignments. The NaY zeolite was equilibrated with NO_2 and propylene (1:1) mixture for 30 min. After evacuating the gas phase, the NaY zeolite was heated for 30 min and cooled back to room temperature before recording each of the spectra shown in Fig. 8.

Adsorption of the NO_2 and propylene mixture results in the formation of several oxygenated and nitrogen-containing organic compounds. As seen in Figs. 7 and 8, adsorbed oxygenated hydrocarbons ($C_xH_yO_z$) with absorptions at 2985, 1723, 1694, 1528, 1508 and 1354 cm^{-1} appear immediately in the spectrum recorded at 298 K. Carbonyl group containing compounds may come about from the direct oxidation of adsorbed propylene by adsorbed NO_x^- [22,41,53]. Two bands at 1528 and 1508 cm^{-1} develop quickly after the co-adsorption of NO_2 and propylene. These have been previously assigned to carbenium ions formed upon adsorption of olefins on acidic zeolites [54]. Since there are no strong Bronsted acid sites in the nanocrystalline NaY zeolite used in our study, these two bands are most likely due to the formation of monodentate carbonate and formate ions, respectively [55].

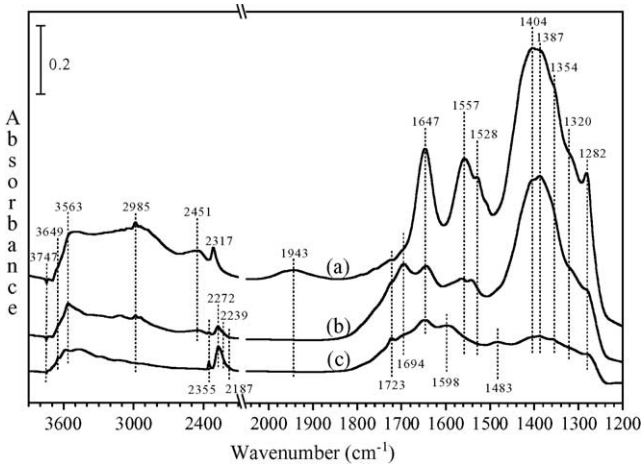

Fig. 8. FT-IR spectra of adsorbed species following adsorption of an NO_2 and propylene (1:1) mixture at (a) 298 K and heating to (b) 373 K and (c) 473 K. All spectra shown in Figs. 8 use the nanocrystalline NaY zeolite prior to adsorption as a reference. In addition, gas-phase absorptions have been subtracted from each of the FT-IR spectra.

These organic compounds may be intermediates or possibly final products in the SCR reaction.

Surface adsorbed NO (1969 cm^{-1}) and N_2O_3 (1943 cm^{-1}) appear upon adsorption of the NO_2 and propylene mixture. These species are stable up to hours at room temperature. However, they disappeared quickly upon heating to 373 K. Another surface species that appears to have similar stability is identified as NCO species on Si^{4+} sites. NCO is identified by the absorption band at 2317 cm^{-1} and has been identified in previous studies using isotope labels [7]. Two surface species characterized by fairly intense absorption bands at 1557 and 1647 cm^{-1} appear to be more thermally stable than NO, N_2O_3 and NCO as these bands persist in the spectra even after heating to 373 K. Yeom et al. investigated the adsorption and reactions of nitromethane in zeolite Y [7]. Based on their isotopic studies, the two intense absorption bands are assigned to organic nitro (1557 cm^{-1}) and nitrito (1647 cm^{-1}) compounds, respectively. Another possible stable intermediate that some consider to be important in the SCR reaction is oxime. Oxime may be responsible for the broad absorbance between 3150 and 3300 cm^{-1} [18].

Most of the absorption bands decreased in intensity after the nanocrystalline NaY zeolite was heated at elevated temperature. Ketones or aldehydes are produced at 373 K as indicated by the band at 1694 cm^{-1} but then convert into other products by heating to 473 K. Surface adsorbed carbon dioxide (2355 cm^{-1}) and isocyanic acid (2272 cm^{-1}) [7] develop in the zeolite upon heating to 373 and 473 K (Fig. 8). At elevated temperature, two other absorption peaks appear in the spectra at 2239 and 2187 cm^{-1} (Fig. 8). These two features have been assigned to organic isocyanate and nitrile in several previous studies using alumina-supported materials as SCR catalysts [19,48–52]. The assignments of isocyanate and nitrile have been supported by other experiments involving NO + CO reactions [50]. Since there is EFAL detected in the nanocrystalline NaY zeolite used in our study, these two absorptions are assigned to organic isocyanate and nitrile adsorbed on EFAL sites. They most likely come from the thermal reaction of organic nitro/nitrito compounds or oxime. Unlike the band at 1557 cm, the absorption at 1647 cm^{-1} persists even after heating to 473 K. This may indicate the formation of a primary amide, which can be generated via the hydrolysis of nitriles and/or thermal reaction of organic nitro/nitrito species. The assignment for the bands at 1598 and 1483 cm^{-1} is difficult since there are numerous literature assignments for bands at these two frequencies and are most likely due to the presence of unsaturated carbonaceous residues or coke [46]. Organic isocyanates and coke are the only compounds adsorbed in NaY zeolite after evacuating the sample overnight at 673 K.

3.4. Low temperature propylene-SCR of NO_2

Propylene-SCR of NO_2 at different temperatures was investigated next. The FT-IR spectra of the gas phase as a func-

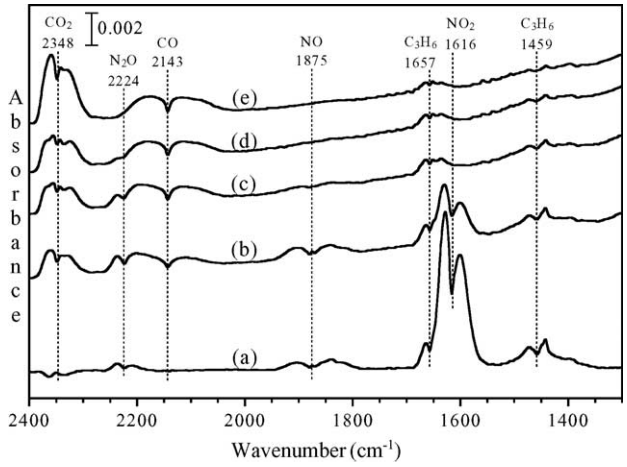

Fig. 9. FT-IR spectra of the gas phase following propylene-SCR of NO_2 in nanocrystalline NaY at 473 K for (a) 0 min, (b) 10 min, (c) 30 min, (d) 1 h and (e) 4 h.

tion of time at a temperature of 473 K is shown in Fig. 9. The concentration of the gases was again calculated from the integrated absorbance of the individual band using the calibration procedure discussed in the experimental section. Fig. 10 shows the amount of the various gaseous species as a function of time in propylene-SCR of NO_2 at 473 K. Immediately after the heating process begins, gaseous NO_2 decreases and is completely gone after 25 min. The concentrations of NO and N_2O initially increase until a maximum is reached at approximately $t = 10$ min, then gradually decrease to zero. Propylene (1459 and 1657 cm^{-1}), CO (2143 cm^{-1}) and CO_2 (2348 cm^{-1}) were the only carbon-containing molecules detected in the gas phase. Although not directly measured, N_2 and O_2 most likely form as well, based on the estimated nitrogen mass balance. Some water is apparent in the gas-phase spectra as well. A similar time course experiment was done at $T = 373$ K. These data are summarized in Table 3 with some additional experiments as well.

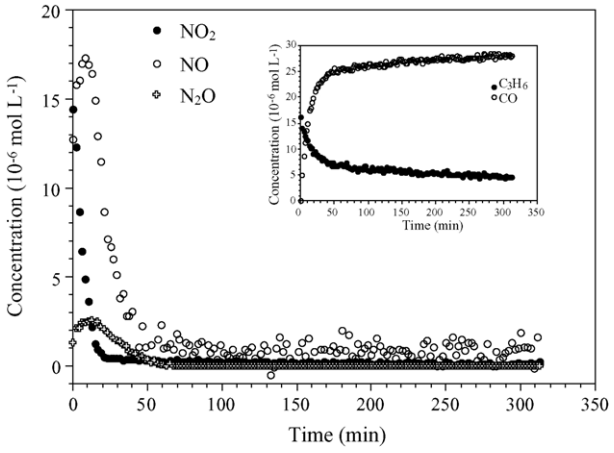

Fig. 10. Evolution of gaseous N-containing species during propylene-SCR of NO_2 in nanocrystalline NaY at 473 K. The inset shows the decay and evolution of propylene and carbon monoxide, respectively. Spectra were recorded every 2 min.

Table 3
Product distribution and conversion of gas-phase NO_2 and adsorbed NO_3^- in propylene-SCR of NO_2 at different temperatures after 6 h of reaction time

Reaction temperature (K)	Product distribution (μmol L^{-1})[a]				%Conversion[b]	
	NO	N_2O	CO	CO_2	NO_2	NO_3^-
298	12.5	3.0	0	0	82	0
373	0	0.4	24.7	1.6	100	3
473	0	0	28.1	8.6	100	29
473[c]	40.9	3.7	6.4	13.9	100	68
473, O_2[d]	25.1	4.6	1.3	40.7	100	87

[a] The total loading of NO_2 was 50 ± 5 μmol L^{-1}; in the absence of oxygen the initial concentration of gas-phase NO_2 after adsorption equilibrium at 298 K was 16 ± 4 μmol L^{-1}.

[b] Conversion of NO_2 refers to the change of NO_2 in gas phase; conversion of NO_3^- describes the change associated with the integrated absorbance in the entire 1230–1600 cm^{-1} spectral region (because of overlapping absorption bands due to other adsorbed species, this estimate could be in error by as much as 20%).

[c] Propylene-SCR of NO_2 was done using a partially deactivated zeolite catalyst (see text for further details).

[d] Propylene-SCR of NO_2 with O_2 present in the IR cell.

Table 3 summarizes the gas-phase product distribution and percent conversion of gas-phase NO_2 and adsorbed nitrate (vide infra) in propylene-SCR of NO_2 at three different temperatures (298, 373 and 473 K). Based on the nitrogen balance, the complete reduction of NO_2 into N_2 and O_2 was found at 473 K after 6 h of reaction. Although a small amount of N_2O existed after 6 h at 373 K, it was expected that it too would disappear with longer reaction time. CO and CO_2 were generated as the major carbon containing products in the gas phase.

It should be pointed out that the conversion of NO_3^- in Table 3 stands for the conversion of species responsible for the absorption bands between 1230 and 1600 cm^{-1}. Even though some of the absorptions in the region are due to other adsorbates, it can still be an approximate measure of how much NO_3^- species reacted since NO_3^- accounts for most of the absorbance in that region (estimated to be ~90%).

Complete conversion of NO_2 did not occur when coke accumulated in the NaY zeolite (referred to as "partially deactivated NaY zeolite" in Table 3). Propylene-SCR of NO_2 at 473 K in a partially deactivated NaY zeolite converted approximately 90% of loaded NO_2 into NO and N_2O. The evolution of NO_2, NO and N_2O with time was similar to that of thermal reduction, except for the higher concentration of N_2O. Compared to SCR reaction in active NaY zeolite, less propylene was consumed, but the CO_2 to CO ratio and conversion of NO_3^- were much higher. More undesired products, i.e. partially oxidized organics, were generated in the zeolite as well. These products include surface adsorbed carbonyl compounds (1723 and 1694 cm^{-1}).

Although an excess amount of oxygen is present under typical lean burn conditions, only propylene and NO_2 were included in the starting reaction mixture in this study for several reasons. First, an intermediacy of NO_2 in SCR of NO has been suggested [6]. Furthermore, the oxidation of propylene

Table 4
Initial reaction rates (10^{-2} μmol L^{-1} s^{-1}) in first 10 min

Reaction temperature (K)	Thermal (NO)	Propylene-SCR		
		NO_2 (loss)	PE (loss)	CO
298	0.1	0.4	0	0
373	1.0	2.1	0.7	2.9
473	2.8	2.0	0.8	2.6
473[a]		0.9	0.3	0.4

[a] Propylene-SCR of NO_2 was done using a partially deactivated zeolite catalyst (see text for further details).

by oxygen competes with the SCR reaction. This is confirmed by the propylene-SCR of NO_2 in nanocrystalline NaY zeolite at 473 K in the presence of oxygen, propylene was found to be consumed within 2 h at 473 K. The concentration of NO reached a maximum and then decreased slowly.

Table 4 summarizes the initial reaction rates in catalytic reduction of NO_2. The initial reaction rates were obtained by linear fitting the concentration of individual gaseous species in the first 10 min of the reaction. NO for thermal reduction, NO_2, propylene and CO for SCR reaction were chosen because their concentration changed monotonically with reaction time. In thermal reduction of NO_2, the initial reaction rates increased with temperature. Propylene-SCR of NO_2 did not occur to any great extent in nanocrystalline NaY zeolite at room temperature. In propylene-SCR of NO_2, the initial reaction rates at 373 K were approximately the same as those at 473 K. This reveals a free radical behavior for the early stage of SCR reactions as the reaction rates are independent of temperature once a certain threshold temperature is reached in which the free radicals are formed. The high CO to CO_2 ratio in Table 3 also suggests a free radical pathway [7].

4. Discussion

4.1. Formation of NO in thermal reduction of NO_2

In earlier studies it was found that the adsorption of NO_2 on ion exchanged Y zeolite occurred preferentially via surface nitrates on exchangeable metal cation sites and partly on cationic EFAL [12]. A second pathway has been proposed involving the reaction between strongly adsorbed water and NO_2 [9,11]. Other studies indicate the possibility that nitrate is formed via two or more different mechanisms that populate different sites [7]. The disproportionation of NO_2 has been suggested to explain the formation of surface species and NO over CuZSM-5 [41]. Underwood and co-workers proposed a mechanism involving the formation of nitrite first followed by nitrate [37].

Based on the experimental observations, the formation of surface nitrate and nitrite in NaY zeolite can be best explained by reactions 1 and 2.

$$2NO_2 + H_2O \rightarrow HNO_3 + HONO \quad (1)$$

$$2NO_2 \rightarrow NO^+ + NO_3^- \quad (2)$$

Reaction 1 is the minor path since only a trace amount of water is left in the zeolite after heating to 673 K under vacuum. However, adsorption of NO_2 happens preferentially via reaction 1 in the presence of water, as indicated by the formation of nitrite (1230 cm^{-1}) in the spectra shown in Fig. 4.

In this study, decomposition of NO_2 should involve the participation of NO_2 from the gas phase. An equilibrium might exist between surface NO_x^- species and gaseous NO_2 (reaction 3). At elevated temperature, NO_2 was released from the NaY zeolite and reacted with surface cationic sites (reaction 4a) or nitrite (reaction 4b). M^{n+} represents Na^+ or EFAL sites.

$$M^{n+} - NO_3^- \rightarrow NO_2 + M^{n+} - O^- \text{(at elevated temperature)} \quad (3)$$

$$M^{n+} + 2NO_2 \rightarrow M^{n+} - NO_3^- + NO \quad (4a)$$

$$M^{n+} - NO_2^- + NO_2 \rightarrow M^{n+} - NO_3^- + NO \quad (4b)$$

The small amount of N_2O produced in thermal reduction of NO_2 might come from the disproportionation of NO [12,38,56]. Significant thermal reduction of NO to N_2O was observed only at temperature above 573 K.

Notably, the concentration of NO reached a maximum at $t = 150$ min and was constant thereafter (Fig. 5). Conversion of surface NO_3^- species increased from 64% at 373 K to 90% at 473 K (Table 1). This means that some of the NO_3^- species are more strongly adsorbed and less reactive. Two different reactivity classes of surface nitrates in zeolite Y have been observed in other studies [7].

4.2. Formation of NO and N_2O in the adsorption of NO_2 and propylene mixture at room temperature

The concentration of NO and N_2O upon adsorption of the NO_2 and propylene mixture (Fig. 10) was consistently higher than that after the adsorption of NO_2 alone (Fig. 5). Surface adsorbed NO and N_2O_3 (1969 and 1943 cm^{-1}, respectively) were observed upon exposure of the mixture to NaY zeolite (Fig. 7), but not in the adsorption of NO_2 alone (Fig. 4).

Although NO^+ was not observed in the adsorption of NO_2 and propylene mixture, it could play an important role due to its low thermal stability and high reactivity. Gerlach et al. studied the reactivity of NO^+ towards propylene over acidic Mordenite [18]. Their study demonstrated that oxime was produced in the reaction between NO^+ and propylene at 393 K and converted into nitrile at higher temperature. In this study, the disappearance of NO^+ by propylene adsorption was observed at room temperature. First the NaY zeolite was equilibrated with NO_2 at room temperature. Then propylene was introduced to NO_2 pre-adsorbed NaY zeolite. NO^+ vanished immediately upon the introduction of propylene. At the same time, surface adsorbed NO and N_2O_3 are observed. Other new surface species observed in adsorption of NO_2 and propylene mixture (Fig. 7) appear within 1 min after adsorp-

tion. The intensity of 1407 cm^{-1} band characterizing surface Na^+-nitrates didn't change significantly. This implies that at $T = 298$ K surface Na^+-nitrate is inactive toward reaction with adsorbed propylene [7].

Thus it is suggested from the data that NO^+ and NO_3^- on EFAL produced upon adsorption of NO_2 (reaction 2) react readily with adsorbed propylene to form NO and organic nitro/nitrito compounds (reactions 5 and 6).

$$NO^+ + CH_3{-}CH{=}CH_2 \rightarrow [CH_3{-}CH{=}CH_2]^+ + NO \quad (5)$$

$$M^{n+} - NO_3^- + [CH_3{-}CH{=}CH_2]^+ \rightarrow C_3H_5NO_2 + M^{n+} - OH \quad (6)$$

The high reactivity of the α-H in propylene and the stabilization of allylic species by cations in zeolite Y could facilitate these two reactions [57,58]. Reaction 6 can lead to the generation of acidic hydroxyl groups. This is consistent with the appearance of a broad band at 3562 cm^{-1} associated with hydroxyl groups on EFAL (Fig. 7). Oxime was then produced in the reaction between NO^+ and adsorbed propylene in presence of the weak Bronsted acidic sites. It is also possible that organic nitro/nitrito compounds came from the direct reaction between adsorbed propylene and certain nitrate species, most likely those attached to EFAL sites populated on the external surface of the nanocrystalline NaY zeolite used in this study.

4.3. Reaction stoichiometry in propylene-SCR of NO_2

In the absence of oxygen, the balanced reaction for complete reduction of NO_2 by propylene can be written either as

$$(9/2)NO_2 + C_3H_6 \rightleftharpoons 3CO_2 + (9/4)N_2 + 3H_2O \quad (7)$$

$$3NO_2 + C_3H_6 \rightleftharpoons 3CO + (3/2)N_2 + 3H_2O \quad (8)$$

assuming CO_2 or CO as the only carbon-containing products, respectively.

As shown in Table 3, a high CO to CO_2 ratio was observed at both 373 and 473 K. Therefore, it can be concluded that the majority of the propylene-SCR of NO_2 in nanocrystalline NaY zeolite occurs via reaction 8 at low temperatures. The concentration of CO_2 was much higher at 473 K than 373 K. This can be easily understood since higher temperature promotes decomposition of oxygenated species and the oxidation of CO to CO_2. The initial reaction rates for NO_2 and CO at both 373 and 473 K are approximately three times that found for propylene (Table 4). Thus, the stoichiometry shown in reaction 8 is in agreement with the measured rate data.

Water was also observed in the gas phase in propylene-SCR of NO_2 at both 373 and 473 K (Fig. 9). However, surface adsorbed water was not present to any great extent in the zeolite after SCR reaction for 6 h. It is most likely that surface adsorbed water was consumed in the hydrolysis of surface species, such as organic nitrile.

It is difficult to write the balanced reaction for propylene-SCR of NO_2 in the presence of excess oxygen because of the multiple reaction pathways involved and the complexities of these reactions. Complete oxidation of propylene by oxygen to CO_2 and water does occur in nanocrystalline NaY zeolite at 473 K. This can be seen by the high CO_2 to CO ratio (Table 3) and the existence of surface adsorbed water after SCR reaction for 6 h. As mentioned previously, NO reduction occurred very slowly once propylene was completely consumed. The low SCR reaction rate is possibly due to a combination of no propylene and the presence of surface adsorbed water. Although oxygen does decrease the zeolite deactivation by oxidizing carbonaceous deposits [6,59], overall it is detrimental to the propylene-SCR of NO_2.

4.4. A mechanism for propylene-SCR of NO_2 at low temperature

Several studies have focused on the mechanism for HC-SCR of NO_x. Most of them have suggested that isocyanate is an important intermediate. The most controversial and least understood aspect of the selective catalytic reduction of NO_2 is the formation of the nitrogen-nitrogen bond which is necessary for the production of N_2. In the SCR reaction over Fe/ZSM-5, isotopic studies have shown that the nitrogen in N_2 comes from both the gas phase NO_x and surface nitrogen-containing species [60]. Radical mechanisms involving azoxy or dinitroso species have been proposed to explain the formation of dinitrogen in zeolites containing transition metals [17,57]. Others have considered –NH complexes as the key intermediate [48]. Recently, Yeom et al. studied the reactions of acetaldehyde, acetic acid and nitromethane with NO_2 on BaNa-Y zeolite [7]. Their study led to the conclusion that the formation of ammonium nitrite (NH_4NO_2) is a crucial step for $DeNO_x$ catalysis. They also suggested a parallel reaction channel involving free radicals to explain reaction pathways which result in a high CO to CO_2 ratio [7].

Based on the observed kinetics and the discussion of the literature above, a mechanism involving free radicals appears to be the most plausible pathway for propylene-SCR of NO_2 in nanocrystalline NaY zeolite. Thermal treatment is necessary for C–H bond dissociation in propylene [61]. At elevated temperature, the SCR reaction is initiated by the abstraction of H from adsorbed propylene to yield the allyl radical, according to reaction 9 [62,63].

$$NO_2 + CH_3{-}CH{=}CH_2 \rightarrow CH_2{-}CH{=}CH_2 + HNO_2 \quad (9)$$

The allylic radical can react with HNO_2 to give oxygenated species and NO (reaction 10).

$$HNO_2 + CH_2{-}CH{=}CH_2 \rightarrow C_3H_6O + NO \quad (10)$$

Upon thermal treatment, surface nitrogen containing compounds (organic nitro/nitrito species and oximes) adsorbed on EFAL sites are converted to nitrile or isocyanate. Acry-

lamide species can be produced via the hydrolysis of organic nitrile or isocyanate. The reaction between acrylamide and HNO_2 (reaction 11) provides one possible pathway for the dinitrogen formation [64,65].

$$RCONH_2 + HNO_2 \rightarrow RCOOH + N_2 + H_2O \quad (11)$$

Another possible channel is the reaction between acrylamide and N_2O_3 in the presence of water.

In propylene-SCR of NO_2, isocyanate radical (2317 cm^{-1}) and isocyanic acid (2272 cm^{-1}) were generated as stable species containing one atom each of nitrogen, carbon and oxygen. Isocyanic acid adsorbed in nanocrystalline NaY zeolite very strongly and can be removed by heating to 573 K under vacuum. It was considered as the precursor of ammonia, which is essential for the formation of dinitrogen [7,66]. In our study, a minor pathway for nitrogen-nitrogen bond formation might involve the reactions of isocyanate radical and isocyanic acid as evidenced by the presence of these species in the FT-IR spectra [51].

5. Conclusions

Catalytic reduction of NO_2 in nanocrystalline NaY zeolite was investigated using in situ transmission FT-IR spectroscopy. NO_2 was stored in the NaY zeolite as nitrate and nitrite. Because of the relatively high external surface area of the nanocrystalline zeolite, there was considerable adsorption on the EFAL sites. Thermal reduction of NO_2 showed high selectivity to NO in the temperature range studied.

In the absence of oxygen, the selective catalytic reduction of NO_2 with propylene at low temperature ($T \leq 473$ K) resulted in complete reduction of NO_2 to N_2 and O_2 in nanocrystalline NaY zeolite. Upon adsorption of propylene and NO_2 mixtures at room temperature, surface organic nitro/nitrite compounds were produced together with other surface species. Isocyanate and nitrile species formed on EFAL sites are found to be important intermediates. Based on kinetic studies, a pathway involving radical reactions appeared to be the most plausible mechanism for the complete reduction of NO_2. In the proposed mechanism, complete reduction of NO_2 was initiated by H abstraction from propylene. The resulting radical, HNO_2, then continues on to form N_2.

Acknowledgements

The authors thank Hassan Alwy for providing the nanocrystalline NaY zeolite sample. Although the research described in this article has been funded wholly or in part by the Environmental Protection Agency through grant number EPA R829600 to SCL and VHG, it has not been subjected to the Agency's required peer and policy review and therefore, does not necessarily reflect the views of the Agency and no official endorsement should be inferred.

References

[1] G. Delahay, B. Coq, Catal. Sci. Ser. 3 (2002) 345.
[2] V.H. Grassian, Int. Rev. Phys. Chem. 20 (2001) 467.
[3] S. Bhattacharyya, R.K. Das, Int. J. Energy Res. 23 (1999) 351.
[4] R. Burch, J.P. Breen, F.C. Meunier, Appl. Catal. B: Environ. 39 (2002) 283.
[5] Y. Traa, B. Burger, J. Weitkamp, Micro. Meso. Mater. 30 (1999) 3.
[6] M. Shelef, Chem. Rev. 95 (1995) 209.
[7] Y.H. Yeom, B. Wen, W.M.H. Sachtler, E. Weitz, J. Phys. Chem. B 108 (2004) 5386.
[8] B. Wen, Y.H. Yeom, E. Weitz, W.M.H. Sachtler, Appl. Catal. B: Environ. 48 (2004) 125.
[9] J. Szanyi, J.H. Kwak, C.H.F. Peden, J. Phys. Chem. B 108 (2004) 3746.
[10] S.J. Schmieg, B.K. Cho, S.H. Oh, Appl. Catal. B: Environ. 49 (2004) 113.
[11] J. Szanyi, J.H. Kwak, R.A. Moline, C.H.F. Peden, Phys. Chem. Chem. Phys. 5 (2003) 4045.
[12] C. Sedlmair, B. Gil, K. Seshan, A. Jentys, J.A. Lercher, Phys. Chem. Chem. Phys. 5 (2003) 1897.
[13] A. Sultana, R. Loenders, O. Monticelli, C. Kirschhock, P.A. Jacobs, J.A. Martens, Angew Chem. Int. Ed. 39 (2000) 2934.
[14] O. Monticelli, R. Loenders, P.A. Jacobs, J.A. Martens, Appl. Catal. B: Environ. 21 (1999) 215.
[15] R. Brosius, J.A. Martens, Top. Catal. 28 (2004) 119.
[16] V.A. Sadykov, V.V. Lunin, V.A. Matyshak, E.A. Paukshtis, A.Y. Rozovskii, N.N. Bulgakov, J.R.H. Ross, Kinet. Catal. 44 (2003) 379.
[17] R.H.H. Smits, Y. Iwasawa, Appl. Catal. B: Environ. L6 (1995) 201.
[18] T. Gerlach, F.W. Schutze, M. Baerns, J. Catal. 185 (1999) 131.
[19] Y. Yu, H. He, Q. Feng, H. Gao, X. Yang, Appl. Catal. B: Environ. 49 (2004) 159.
[20] M. Haneda, Y. Kintaichi, M. Inaba, H. Hamada, Catal. Today 42 (1998) 127.
[21] T. Tanaka, T. Okuhara, M. Misono, Appl. Catal. B: Environ. 4 (1994) L1.
[22] A. Satsuma, T. Enjoji, K. Shimizu, K. Sato, H. Yoshida, T. Hattori, J. Chem. Soc., Faraday Trans. 94 (1998) 301.
[23] W. Song, G. Li, V.H. Grassian, S.C. Larsen, Environ. Sci. Tech. (2004), in press.
[24] S.C. Larsen, V.H. Grassian, in: J.A. Schwarz, C.I. Contescu, K. Putyera (Eds.), Encyclopedia of Nanoscience and Nanotechnology, Marcell Dekker Publishing Co., NY, 2004, 1137.
[25] Q. Li, D. Creaser, J. Sterte, Chem. Mater. 14 (2002) 1319.
[26] W. Song, R.E. Justice, C.A. Jones, V.H. Grassian, S.C. Larsen, Langmuir 20 (2004) 4696.
[27] G. Li, M. Xu, S.C. Larsen, V.H. Grassian, J. Mol. Catal. A: Chem. 194 (2003) 169.
[28] H.G. Karge, Micro. Meso. Mater. 22 (1998) 547.
[29] S. Khabtou, T. Chevreau, J.C. Lavalley, Micro. Mater. 3 (1994) 133.
[30] P.O. Fritz, J.H. Lunsford, J. Catal. 118 (1989) 85.
[31] Y. Xiang, S.C. Larsen, V.H. Grassian, J. Am. Chem. Soc. 121 (1999) 5063.
[32] F. Thibault-Starzyk, B. Gil, S. Aiello, T. Chevreau, J. Gilson, Micro. Meso. Mater. 67 (2004) 107.
[33] M.R. Basila, T.R. Kantner, K.H. Rhee, J. Phys. Chem. 68 (1964) 3197.
[34] A.L. Goodman, E.T. Bernard, V.H. Grassian, J. Phys. Chem. A 105 (2001) 6443.
[35] K.I. Hadjiivanov, Catal. Rev. Sci. Eng. 42 (2000) 71.
[36] A.L. Goodman, T.M. Miller, V.H. Grassian, J. Vacuum Sci. Tech. A 16 (1998) 2585.
[37] A.L. Goodman, G.M. Underwood, V.H. Grassian, J. Phys. Chem. A 103 (1999) 7217.
[38] C.C. Chao, J.H. Lunsford, J. Am. Chem. Soc. 93 (1971) 71.
[39] C.C. Chao, J.H. Lunsford, J. Am. Chem. Soc. 93 (1971) 6794.

[40] K. Hadjiivanov, J. Saussey, J.L. Freysz, J.C. Lavalley, Catal. Lett. 52 (1998) 103.
[41] K. Hadjiivanov, D. Klissurski, G. Ramis, G. Busca, Appl. Catal. B: Environ. 7 (1996) 251.
[42] S.V. Gerei, E.V. Rozhkova, Y.B. Gorokhovatskii, J. Catal. 28 (1973) 341.
[43] B.A. Morrow, I.A. Cody, J. Chem. Soc., Faraday Trans. 1 (71) (1975) 1021.
[44] F. Solymosi, T.J. Bansagi, J. Catal. 156 (1995) 75.
[45] V.H. Grassian, J. Phys. Chem. A 106 (2002) 860.
[46] J.M. Garcia-Cortes, J. Perez-Ramirez, J.N. Rouzaud, A.R. Vaccaro, M.J. Illan-Gomez, C. Salinas-Martinez De Lecea, J. Catal. 218 (2003) 111.
[47] A.L. Smith, Applied Infrared Spectroscopy: Fundamentals, Techniques, and Analytical Problem Solving, 1979.
[48] M. Haneda, N. Bion, M. Daturi, J. Saussey, J. Lavalley, D. Duprez, H. Hamada, J. Catal. 206 (2002) 114.
[49] Y. Ukisu, S. Sato, A. Abe, K. Yoshida, Appl. Catal. B: Environ. 2 (1993) 147.
[50] G.R. Bamwenda, A. Ogata, A. Obuchi, J. Oi, K. Mizuno, J. Skrzypek, Appl. Catal. B: Environ. 6 (1995) 311.
[51] W. Schiesser, H. Vinek, A. Jentys, Appl. Catal. B: Environ. 33 (2001) 263.
[52] S. Sumiya, H. He, A. Abe, N. Takezawa, K. Yoshida, J. Chem. Soc., Faraday Trans. 94 (1998) 2217.
[53] K. Hadjiivanov, L. Dimitrov, Micro. Meso. Mater. 27 (1999) 49.
[54] I. Kiricsi, H. Foerster, G. Tasi, J. Mol. Catal. 65 (1991) L29.
[55] T.E. Hoost, K.A. Laframboise, K. Otto, Appl. Catal. B: Environ. 7 (1995) 79.
[56] T. Weingand, S. Kuba, K. Hadjiivanov, H. Knoezinger, J. Catal. 209 (2002) 539.
[57] N.W. Hayes, R.W. Joyner, E.S. Shpiro, Appl. Catal. B: Environ. 8 (1996) 343.
[58] T. Beutel, B. Adelman, W.M.H. Sachtler, Catal. Lett. 37 (1996) 125.
[59] J.L. d'Itri, W.M.H. Sachtler, Appl. Catal. B: Environ. 2 (1993) L7.
[60] H.Y. Chen, T. Voskoboinikov, W.M.H. Sachtler, J. Catal. 186 (1999) 91.
[61] E. Finocchio, G. Busca, V. Lorenzelli, R.J. Willey, J. Catal. 151 (1995) 204.
[62] J. Vassallo, E. Miro, J. Petunchi, Appl. Catal. B: Environ. 7 (1995) 65.
[63] A.D. Cowan, R. Duempelmann, N.W. Cant, J. Catal. 151 (1995) 356.
[64] P.A.S. Smith, The Organic Chemistry of Open-Chain Nitrogen Compounds, vol. I, 1965.
[65] H.Y. Chen, T. Voskoboinikov, W.M.H. Sachtler, J. Catal. 180 (1998) 171.
[66] N.W. Cant, D.C. Chambers, A.D. Cowan, I.O. Liu, A. Satsuma, Top. Catal. 10 (2000) 13.